

# 1 The Telomere Length Landscape of Localized 2 Prostate Cancer

3  
4 Julie Livingstone<sup>1,2,3,4</sup>, Yu-Jia Shiah<sup>5</sup>, Takafumi N. Yamaguchi<sup>1,2,3,4</sup>, Lawrence E.  
5 Heisler<sup>5</sup>, Vincent Huang<sup>5</sup>, Robert Lesurf<sup>5</sup>, Erik Drysdale<sup>5</sup>, Jeffrey Green<sup>5</sup>, Theodorus  
6 van der Kwast<sup>6,7</sup>, Robert G. Bristow<sup>6,8,9</sup>, Michael Fraser<sup>6</sup>, Paul C. Boutros<sup>1,2,3,4,8,10</sup>

7 <sup>1</sup> Department of Human Genetics, University of California, Los Angeles, CA 90095, USA

8 <sup>2</sup> Department of Urology, University of California, Los Angeles, CA 90024, USA

9 <sup>3</sup> Jonsson Comprehensive Cancer Centre, University of California, Los Angeles, CA 90024, USA

10 <sup>4</sup> Institute for Precision Health, University of California, Los Angeles, CA 90024, USA

11 <sup>5</sup> Ontario Institute for Cancer Research, Toronto, ON M5G 0A3, Canada

12 <sup>6</sup> Princess Margaret Cancer Centre, University Health Network, Toronto, ON M5G 2M9, Canada

13 <sup>7</sup> Department of Pathology, Laboratory Medicine Program, University Health Network, Toronto, ON M5G  
14 2C4, Canada

15 <sup>8</sup> Department of Medical Biophysics, University of Toronto, Toronto, ON M5G 1L7, Canada

16 <sup>9</sup> Manchester Cancer Research Centre, Manchester, United Kingdom

17 <sup>10</sup> Department of Pharmacology and Toxicology, University of Toronto, Toronto, ON M5S 1A8, Canada

18  
19 **Corresponding Author:** Dr. Paul C. Boutros, 12-109 CHS; 10833 Le Conte Avenue;  
20 Los Angeles, CA 90095. Phone: 310-794-7160; Email: [pboutros@mednet.ucla.edu](mailto:pboutros@mednet.ucla.edu)

21 **Keywords:** Telomere length; prostate cancer; genomic instability; integration

22 **Word Count of the text:** 3,618 (excluding references)

23 **Word Count of the abstract:** 160

## 24 **Abstract**

25 Replicative immortality is a hallmark of cancer, and can be achieved through telomere  
26 lengthening and maintenance. We report telomere lengths (TLs) of 392 localized  
27 prostate cancer tumours and characterize their relationship to genomic, transcriptomic  
28 and proteomic features. Shorter tumour TLs were associated with elevated genomic  
29 instability, including single-nucleotide variants, indels and structural variants. Genes  
30 involved in cell proliferation and signaling were correlated with tumour TL at all levels of  
31 the central dogma. TL was also associated with multiple clinical features of a tumour.  
32 Longer TLs in non-tumour (blood) samples were associated with a lower rate of  
33 biochemical relapse after definitive local therapy. Our analysis integrates multi-omics  
34 data to illuminate the relationship of specific genomic alterations in a tumour and TL in  
35 prostate cancer. Although the role of telomere length in cancer has been well studied,  
36 its association to genomic features is less well known. We describe the multi-level  
37 integration of telomere length, genomics, transcriptomics and proteomics in localized  
38 prostate cancer. **Patient Summary** We examined the association between telomere  
39 length and multiple omics-level data in prostate cancer. We observed that traditional  
40 telomere mutations are rare in prostate cancer and that telomere length is associated  
41 with multiple measure of genomic instability.

## 42 Introduction

43 Telomeres, which make up the ends of chromosomes, consist of a repeat TTAGGG  
44 sequence<sup>1</sup> along with bound proteins known as shelterin<sup>2</sup>. Telomeres protect  
45 chromosomal ends from degradation by the DNA double-strand break (DSB) response  
46 pathway. Due to the linearity of chromosomes and chromosomal replication, telomeres  
47 are shortened by approximately 50 bp during mitosis<sup>3</sup>. When telomeres become  
48 substantially shortened, cell cycle progression halts and cells enter replicative  
49 senescence; further replication leads to cellular crisis and eventually cell death<sup>4</sup>.  
50 Telomere maintenance and lengthening is essential for cancer cell proliferation and  
51 enables replicative immortality: a fundamental hallmark of cancer<sup>5</sup>. Telomere regulation  
52 occurs through two known mechanisms: activation of telomerase or alternative  
53 lengthening of telomeres (ALT) which relies on homology-directed DNA replication<sup>6</sup>.

54 Despite the pan-cancer studies analyzing the telomere length from various tumour  
55 types<sup>7,8</sup>, the role of telomere maintenance in individual tumour types is poorly  
56 understand. Moreover, the relationship between telomere length and biologically-  
57 relevant genomic indices, such as percentage of the genome altered (PGA; <sup>9,10</sup>, and  
58 other measures of mutational density has not been assessed, nor has the association  
59 between telomere length and clinical outcome in prostate cancer.

60 We and others have described the genomic, transcriptomic and proteomic landscape of  
61 localized, non-indolent prostate cancer<sup>11-17</sup>: the most frequently diagnosed non-skin  
62 malignancy in North American men (~250,000 new cases per year). Localized prostate  
63 cancer is a C-class tumour<sup>18</sup>, characterized by a paucity of driver single nucleotide  
64 variants (SNVs) and a relatively large number of structural variants (SVs), including  
65 copy number aberrations (CNAs) and genomic rearrangements (GRs). Several of these  
66 aberrations, including mutations in *ATM* and amplifications of *MYC* – which drive DSB  
67 repair and cell proliferation, respectively – are associated with significantly reduced time  
68 to biochemical and metastatic relapse after local therapy<sup>19</sup>. Intriguingly, both of these  
69 mutations have also been associated with telomere maintenance<sup>20,21</sup> and telomere  
70 shortening – relative to adjacent epithelium<sup>22</sup>. Similarly an interaction between hypoxia,  
71 dysregulated *PTEN*, *TERT* abundance and telomere shortening was recently  
72 illustrated<sup>14</sup>. Despite this, no well-powered study exists evaluating the association  
73 between telomere length, somatic features and clinical outcome in prostate cancer.

74 To fill this gap, we quantify the telomere length and somatic mutational landscapes of  
75 392 localized prostate tumours. We explore associations between telomere length and  
76 the tumour methylome, transcriptome and proteome. Using rich clinical annotation, we  
77 further assessed the relationship between telomere length and outcome. Taken  
78 together, these data establish the role and regulation of telomere length in localized  
79 prostate cancer, and establish clear links between telomere maintenance and drivers of  
80 prostate cancer development and clinical aggression.

## 81 Results

### 82 Association of telomere length with somatic nuclear driver events

83 To investigate the impact of telomere length (TL) on the clinico-genomics of prostate  
84 tumours, we exploited whole genome sequencing (WGS) of 392 published tumour-  
85 blood pairs<sup>13–16</sup>. We estimated both tumour and non-tumour (blood) TLs for each  
86 sample using TelSeq v0.0.1<sup>23</sup> and TelomereHunter<sup>24</sup>. After quality control, 381 samples  
87 were retained for further analysis (see **Methods**). All tumours were treatment-naive,  
88 and detailed clinical information was collected and is available in **Supplementary**  
89 **Table S1**. The cohort consisted of 11% ISUP Grade Group (GG) 1, 52% GG2, 33.5 %  
90 GG3, 6.8% GG4 and 3.4% GG5. For the majority of samples, the tumour was confined  
91 to the prostate (6.5% T1, 53.0% T2, 40.0% T3, 0.5% T4). The mean tumour coverage  
92 was  $73.1x \pm 20.6x$ ; the mean non-tumour (blood) coverage was  $44.1x \pm 13.4x$ . Median  
93 clinical follow-up time was 7.46 years. TLs for each sample, along with clinical and  
94 genomic summary data are in **Supplementary Table S1**. Non-tumour (blood) TLs  
95 varied dramatically across individuals, ranging from 2.10 kbp to 15.0 kbp, with a median  
96 of  $4.52 \pm 1.35$  kbp. By contrast, tumour TLs varied less but were significantly shorter,  
97 ranging from 1.03 kbp to 6.45 kbp with a median of  $3.36 \pm 0.87$  kbp. Non-tumour (blood)  
98 TLs were not associated with sequencing coverage (**Supplementary Fig. S1A**).  
99 Tumour TLs were independent of tumour purity but there was a weak negative  
100 correlation between coverage and TL driven by some samples sequenced with over  
101 100x coverage (**Fig. 1D**; **Supplementary Figs. 1A-B**). Tumour and non-tumour (blood)  
102 TLs estimates from TelSeq and TelomereHunter were highly correlated  
103 (**Supplementary Fig. S1C**). To account for batch effects, a linear model was fit and TLs  
104 were adjusted (**Supplementary Figs. S1D-E**). TL ratios (tumour TL / non-tumour  
105 (blood) TL) were calculated to further reduce any effects caused by co-founding of age  
106 at diagnosis. Tumour and non-tumour (blood) TLs were positively correlated with one  
107 another ( $\rho = 0.37$ ,  $P = 7.30 \times 10^{-14}$ , **Fig. 1A**). As expected, TL ratio was positively  
108 correlated with tumour TL ( $\rho = 0.63$ ,  $P < 2.2 \times 10^{-16}$ ; **Fig. 1B**) but negatively correlated  
109 with non-tumour (blood) TLs ( $\rho = -0.40$ ,  $P < 2.2 \times 10^{-16}$ ; **Figs. 1C**).

110 To assess whether tumour TL was related to any specific genomic property of a tumour,  
111 we evaluated a set of driver mutations previously identified in prostate cancer<sup>13</sup>. The  
112 relationship of each of these features with tumour TL is shown in **Fig. 1D**. While tumour  
113 TL was not associated with any known prostate cancer-related genomic rearrangement  
114 (GR) or single nucleotide variant (SNV) at current statistical power, samples with *CHD1*,  
115 *RB1* or *NKX3-1* deletions had shorter tumour TL (**Fig. 1D**). By contrast, TL was closely  
116 associated with multiple measures of genomic instability. Tumours with shorter TLs had  
117 an elevated number of SNVs ( $\rho = -0.27$ ,  $P = 5.78 \times 10^{-8}$ ; **Fig. 2A**), indels ( $\rho = -0.32$ ,  $P =$   
118  $2.83 \times 10^{-10}$ ; **Fig. 2C**) and GRs ( $\rho = -0.12$ ,  $P = 1.6 \times 10^{-2}$ ; **Fig. 2E**), as well as higher

119 PGA ( $\rho = -0.21$ ,  $P = 3.95 \times 10^{-5}$ ; **Fig. 2G**), suggesting tumours with shorter telomeres  
120 accrue more mutations of all types without strong selective pressures for specific ones.

121 To determine whether these associations with somatic features were also related to an  
122 individual's non-tumour (blood) cells, we related each somatic feature against the TL  
123 ratio (tumour TL / non-tumour (blood) TL). Similar to tumour TL, the TL ratio did not  
124 significantly differ between samples with any of the recurrent prostate cancer-related  
125 GRs or CNAs but samples with a somatic SNV in the gene *SPOP* had smaller TL ratios  
126 (**Supplementary Fig. S2**). We identified significant correlations between somatic  
127 genomic instability measures and TL ratio. Tumours with an elevated number of SNVs  
128 ( $\rho = -0.15$ ,  $P = 4.20 \times 10^{-3}$ ; **Fig. 2B**), indels ( $\rho = -0.18$ ,  $P = 2.97 \times 10^{-4}$ ; **Fig. 2D**), GRs ( $\rho$   
129  $= -0.22$ ,  $P = 1.08 \times 10^{-5}$ ; **Fig. 2F**) and PGA ( $\rho = -0.13$ ,  $P = 1.69 \times 10^{-2}$ ; **Fig. 2H**) had  
130 smaller TL ratios.

131 We also assessed the association of telomere length with chromothripsis using  
132 published ShatterProof<sup>25</sup> scores from a subset of samples in this cohort ( $n = 170$ )<sup>13</sup>.  
133 There was no association between scores representing chromothripsis events in either  
134 tumour TL ( $\rho = 0.06$ ,  $P = 0.43$ ) or TL ratio ( $\rho = 0.02$ ,  $P = 0.80$ ).

### 135 **Fusion events are associated with telomere length**

136 When telomeres shorten beyond a certain length, double strand break repair is  
137 activated and cell cycle progression is arrested *via* the *TP53* pathway<sup>26</sup>. Failure to block  
138 cell growth can lead to telomere crisis and subsequent translocations, chromothripsis or  
139 chromosome fusions<sup>27</sup>. We explored the association of TL and the number of gene  
140 fusions present in a tumour. There was a negative correlation between the number of  
141 gene fusions and tumour TL ( $\rho = -0.26$ ;  $P = 2.18 \times 10^{-3}$ ) but no correlation with TL ratio  
142 (**Figs. 2I-J**). In a previous study, 47 recurrent gene fusions were discovered from  
143 matched RNA-Sequencing data<sup>17</sup>. Differences in tumour TL and TL ratio between  
144 samples with a gene fusion and those without were investigated for each of these  
145 recurrent fusions. No gene fusions were associated with TL ratio, but *PCAT1:CASC21*  
146 gene fusion was significantly associated with tumour TL (Mann Whitney U test;  $Q = 2.07$   
147  $\times 10^{-4}$ ; **Supplementary Fig. S3** and **Supplementary Table S2**). Tumours with this  
148 fusion had shorter tumour telomeres (mean = 3.3 kbp) than those without (mean = 3.8  
149 kbp). These data suggest that the number of fusions and specifically the long non-  
150 coding RNA *PCAT1*, which promotes cell proliferation, is related to tumour TL.

### 151 **The role of *TERT* in prostate cancer**

152 A pan-cancer study reported that *TERT* alterations including promoter mutations,  
153 amplifications and structural variants were seen in approximately 30% of all cancers<sup>7</sup>. In  
154 our cohort, 10% of samples had *TERT* amplifications, 11% had *TERC* amplifications,  
155 ~1% had *TERT* structural variants and no samples had *TERT* SNVs or gene fusions.  
156 *TERT* mutations were seen less frequently in other localized prostate cancer datasets,  
157 1.7% (17/1,013; <sup>28</sup> and 0.6% (2/333; <sup>12</sup>), and in a metastatic dataset 3% (5/150; <sup>19</sup>, likely

158 reflecting the early-stage of our cohort. Mutations in *ATRX* and *DAXX*, which have been  
159 correlated with longer telomeres<sup>29</sup>, were rare in our cohort: only two samples harboured  
160 a CNA in *DAXX*, and only four samples had an alteration in *ATRX*.

161 Tumour *TERT* RNA abundance was not correlated with tumour TL or TL ratio (**Fig. 3A**).  
162 Samples with higher *TERT* RNA abundance had fewer GRs ( $\rho = -0.17$ ;  $P = 4.79 \times 10^{-2}$ ;  
163 **Fig. 3B**), but there was no correlation between *TERT* abundance and SNV count ( $\rho = -$   
164  $0.04$ ,  $P = 0.67$ ; **Fig. 3C**), indel count ( $\rho = -0.04$ ,  $P = 0.132$ ; **Fig. 3D**) or PGA ( $\rho = -0.13$ ,  $P$   
165  $= 0.679$ ; **Fig. 3E**). The abundance of *TERC*, the telomerase RNA component, was  
166 negatively correlated with tumour TL ( $\rho = -0.24$ ;  $P = 4.55 \times 10^{-3}$ ; **Supplementary Fig.**  
167 **4A**) but there was no correlation with TL ratio or GR count ( $\rho = 0.12$ ;  $P = 0.145$ ;  
168 **Supplementary Fig. 4B**). *TERC* abundance was positively correlated with SNV count  
169 ( $\rho = 0.23$ ;  $P = 7.34 \times 10^{-3}$ ; **Supplementary Fig. 4C**), indel count ( $\rho = 0.34$ ;  $P = 4.88 \times$   
170  $10^{-5}$ ; **Supplementary Fig. 4D**) and PGA ( $\rho = 0.26$ ;  $P = 1.90 \times 10^{-3}$ ; **Supplementary Fig.**  
171 **4E**). *TERT* and *TERC* abundances were not correlated ( $\rho = 0.02$ ;  $P = 0.794$ ). These  
172 data suggest that *TERT* signaling is not significantly abrogated in localized prostate  
173 cancer either by somatic aberrations or through gene expression changes.

174 To explore the relationship of *TERT* RNA abundance and tumour TL further, we  
175 considered known activating transcription factors. Transcription of *TERT* can be  
176 activated by *MYC* and *SP1* and repressed by *AR*<sup>30</sup>. *MYC* amplifications occur in 14.5%  
177 of our samples (51/351; **Fig. 1D**), while *SP1* CNAs are rare (3/351). *TERT* and *MYC*  
178 mRNA abundance was positively correlated ( $\rho = 0.27$ ;  $P = 1.46 \times 10^{-3}$ ) but *MYC*  
179 abundance was unrelated to tumour TL (**Supplementary Fig. S5A**). Contrastingly,  
180 there was a positive correlation between tumour TL length and *SP1* abundance ( $\rho =$   
181  $0.23$ ;  $P = 6.84 \times 10^{-3}$ ) but no significant correlation between *SP1* and *TERT* abundance  
182 (**Supplementary Fig. S5B**). We did not observe any statistically significant correlations  
183 between *AR* and *TERT* abundance, or tumour TL (**Supplementary Fig. S5C**). The  
184 direct relationship of these transcription factors on *TERT* is hard to elucidate because of  
185 the low measured abundance of *TERT*. Nonetheless, the abundance of *SP1* and *AR*  
186 appear to positively and negatively affect tumour TL, respectively.

187 To determine whether *TERT* was being regulated epigenetically, first investigated the  
188 correlation between its methylation status and its RNA abundance. We identified one  
189 CpG with a significant negative correlation and two with positive correlations  
190 (Spearman's correlation;  $P < 0.05$ ;  $|\rho| > 0.2$ ; **Fig. 3F**). Further, 31% (28/91) of *TERT*  
191 CpGs probes were significantly correlated to telomere length: 7 positively and 21  
192 negatively (Spearman's correlation;  $FDR < 0.05$ ;  $|\rho| > 0.2$ ; **Fig. 3F**). This strongly  
193 suggests that methylation of *TERT* may impact *TERT* abundance and tumour TL.

## 194 **Candidate regulators of prostate tumour telomere length**

195 Evidence of correlation between methylation and tumour TL in *TERT* led us to  
196 investigate the role of methylation on TL genome-wide. For each gene, we considered

197 the CpG most associated to its mRNA abundance (see **Methods**) and related that to  
198 tumour TL (n = 241). Methylation of almost half of all genes (46%; 7,088/15,492) was  
199 significantly correlated with tumour TL (Spearman's correlation; FDR < 0.05;  
200 **Supplementary Table S3**). Similarly, almost a third of genes showed transcriptional  
201 profiles associated with tumour TL (32%; 4,500/13,958) and 9.3% showed proteomic  
202 correlations (n = 548/5,881; Spearman's correlation; P < 0.05). There were 112 genes  
203 with methylation, transcription and proteome correlations to telomere length.  
204 Remarkably, these showed no functional enrichment. Several genes showed  
205 methylation positively correlated with tumour TL but negatively correlated with RNA and  
206 protein abundance (**Fig. 4A**), suggesting suppression of tumour TL elongation. One  
207 such gene is the oncogene *AKT1*, which regulates processes including cell proliferation,  
208 survival and growth<sup>31</sup>. High *AKT1* abundance may indicate an elevated proliferation and  
209 therefore shorter telomeres.

210 We also identified genes whose methylation was negatively correlated with tumour TL  
211 but positively correlated with RNA and protein abundance suggesting promotion of  
212 telomere elongation (**Fig. 4B**). These included *SLC14A1*, a membrane transporter that  
213 mediates urea transport, and *ITGA3*, an integrin that functions as a cell surface  
214 adhesion molecule. We used g:Profiler<sup>32</sup> to identify 12 pathways enriched in genes that  
215 showed an association with tumour TL (n = 2,768) by methylation and RNA, including  
216 proliferation and immune processes (**Supplementary Fig. S6**).

217 We similarly investigated whether TL ratio was associated with methylation and found  
218 that the methylation levels of 33.7% (5,218/15,492) of genes were significantly  
219 correlated with TL ratio (Spearman's correlation; FDR < 0.05; **Supplementary Table**  
220 **S4**). Surprisingly, fewer than 1% (n = 53/13,958) of genes with overlapping data also  
221 had a significant correlation between RNA abundance and TL ratio and none between  
222 protein abundance and TL ratio (Spearman's correlation; FDR < 0.05). These results  
223 suggest that tumour TL, not TL ratio, is associated with tumour gene expression.

## 224 **Association of telomere length and specific copy number aberrations**

225 Since prostate tumour gene-expression and clinical behaviour is predominantly driven  
226 by CNAs<sup>13,18</sup> we next investigated their role in TL. As noted above (**Fig. 1D**), driver  
227 CNAs were largely unassociated with tumour TL (**Fig. 5A**; white background) or TL ratio  
228 (**Fig. 5B**; white background). We therefore considered copy number changes genome-  
229 wide for associations with TL. We identified 24 loci encompassing 35 genes in which  
230 there was a significant difference in tumour TL in samples with a copy number change  
231 compared to those without (Mann-Whitney U test; FDR < 0.05; **Supplementary Table**  
232 **S5** and **Fig. 5A**). We also identified 128 loci encompassing 319 genes in which there  
233 was an association between copy number status and TL ratio (Mann-Whitney U test,  
234 FDR < 0.05; **Supplementary Table S7**). For example, tumours with deletions in DNA  
235 methyltransferase 1, *DNMT1*, had smaller TL ratios (Q = 0.028, effect size = 0.11, **Fig.**

236 **5B**). An opposing trend was seen in the chromatin organization gene, *PRDM16* ( $Q =$   
237  $0.027$ , effect size =  $0.15$ ) and the membrane metallo-endopeptidase gene, *MMEL1* ( $Q =$   
238  $0.027$ , effect size =  $0.14$ ; **Fig. 5B**), where amplifications resulted in smaller TL ratios.  
239 This analysis highlights that copy number aberrations are more associated with TL ratio  
240 (change in length from non-tumour (blood) TL to tumour TL) than absolute tumour TL.

241 We also explored CNAs in genes comprising the telomere complex (*TERF1*, *TERF2*,  
242 *TERF2IP*, and *POT1*), shelterin interacting proteins (*PINX1* and *RTEL1*), and the  
243 components of telomerase (*TERT* and *TERC*). There were no differences in the tumour  
244 TL (**Supplementary Fig. S7A**) or TL ratio (**Supplementary Fig. S7B**) between samples  
245 with and without a CNA in these genes.

246 Next, we compared TL across previously identified CNA subtypes. There was no  
247 difference in tumour TL ( $P = 0.530$ ; one-way ANOVA) or TL ratio ( $P = 0.778$ ; one-way  
248 ANOVA) in the four CNA subtypes identified from aCGH arrays and associated with  
249 prognosis<sup>9</sup> (**Supplementary Fig. 8A-B**). There was an association between TL ratio  
250 and the six CNA subtypes ( $P = 2.12 \times 10^{-2}$ ; one-way ANOVA) identified from 284  
251 OncoScan SNP arrays<sup>13</sup> but not with tumour TL (**Supplementary Fig. 8C-D**). Samples  
252 in subtype C5, which was defined by amplifications in genes near the end of  
253 chromosomes had smaller TL ratios than C3 (defined by an 8p deletion and an 8q  
254 amplification) and C4 (defined as having a quiet CNA profile). A smaller TL ratio in the  
255 samples from subtype C5 indicates that the non-tumour (blood) TL length was longer  
256 than in the tumour TL (**Supplementary Fig. 8E**): the consequences of this remain to be  
257 elucidated.

## 258 **Clinical correlates of telomere length**

259 The clinical features of a tumour can have prognostic value, and have been associated  
260 with the genomic features of tumours<sup>13</sup>. Higher serum abundance of prostate specific  
261 antigen (PSA), higher ISUP Grading and tumour size and extent are all associated with  
262 worse outcome. Therefore, we considered whether there was interplay between TL and  
263 the clinical features of a tumour. Tumour TL was not significantly correlated to age, ( $\rho =$   
264  $-0.10$ ,  $P = 5.8 \times 10^{-2}$ ; **Fig. 6A**) but there was a significant positive correlation between  
265 age at diagnosis and TL ratio ( $\rho = 0.11$ ,  $P = 2.53 \times 10^{-2}$ ; **Fig. 6B**). Tumour TL was  
266 shorter than non-tumour (blood) TL in younger patients. This could be related to the  
267 aggressiveness of early onset prostate cancers, which is characteristic of tumours in  
268 younger men<sup>33</sup>. There was a negative correlation between pre-treatment PSA levels  
269 between both tumour TL ( $\rho = -0.16$ ,  $P = 2.23 \times 10^{-3}$ ) and TL ratio ( $\rho = -0.19$ ,  $P = 1.70 \times$   
270  $10^{-4}$ ; **Figs. 6C-D**). Neither tumour TL nor TL ratio was associated with ISUP Grade  
271 (**Figs. 6E-F**). Surprisingly, tumour TL was shorter in smaller tumours (T1) than larger  
272 tumours (T2 or T3; one-way ANOVA,  $P = 2.2 \times 10^{-2}$ ; **Fig. 6G**) but this can be explained  
273 by the higher average age of patients with T1 tumours (mean =  $71.3$ ) compared to other



274 T categories (mean = 62.0). Accordingly, there was no association between TL ratio,  
275 which controls for patient age, and T category ( $P = 0.29$ ; **Fig. 6H**).

276 Telomerase activity and TL has been proposed to have clinical utility at three different  
277 stages; diagnosis, prognosis and treatment<sup>30</sup>. TL from biopsies has been correlated with  
278 progression to metastasis and disease specific death<sup>34</sup>. As well, TL from leukocytes has  
279 been associated with poor survival<sup>35,36</sup>. We explored if tumour TL, non-tumour (blood)  
280 TL or TL ratio were associated with biochemical relapse (BCR), an early surrogate  
281 endpoint in intermediate-risk prostate cancer. Cox proportional hazards (Cox PH)  
282 models were fit, splitting patients ( $n = 290$ ) into two groups based on their TL with  
283 increasing cutoff thresholds (50 bp each time; **Supplementary Fig. S9**). From this  
284 outcome-oriented optimal cut-point analysis we discovered that samples with non-  
285 tumour (blood) TL less than 3.9 kbp had a higher rate of BCR than samples with longer  
286 TLs (HR = 2.02,  $P = 1.6 \times 10^{-3}$ ; **Fig. 6I**). Non-tumour (blood) TL is associated with  
287 survival independent of PGA (Cox PH model,  $P = 0.02$ ). There was no association  
288 between tumour TL and BCR (**Fig. 6J**), but there was an association between TL ratio  
289 and BCR, where samples with a TL ratio greater than 0.65 had a lower rate of BCR  
290 (HR = 0.42,  $P = 2.6 \times 10^{-3}$ ; **Fig. 6K**). We also considered TL as a continuous  
291 measurement and fit Cox PH models using tumour TL, non-tumour (blood) TL and TL  
292 ratio. Again, there was no association between continuous tumour TL and BCR but  
293 there was an association between non-tumour (blood) TL (HR = 0.768,  $P = 0.014$ ) and  
294 TL ratio (HR = 1.71,  $P = 0.031$ ; **Supplementary Fig. 9D**). These results suggest that  
295 non-tumour (blood) TL and TL ratio are weakly prognostic, and thus may reflect host  
296 factors that may influence patient risk categorization.

## 297 Discussion

298 These data emphasize the relationship of genomic instability and TL. Genomic  
299 instability has previously been linked with poor outcome in prostate cancer<sup>9,13</sup> and TL  
300 shortening could be the cause of some of this instability. Telomere shortening has been  
301 implicated as an early event in prostate cancer due to evidence of shortened telomeres  
302 observed in a precursor histopathology, high-grade prostatic intraepithelial  
303 neoplasia<sup>37,38</sup>. Since cellular proliferation in prostate cancer is increased by seven fold  
304 compared to normal prostatic epithelial cells<sup>30</sup>, telomeres in these dividing cells will  
305 shorten with each cell division. There is no evidence that primary prostate cancer  
306 exhibits ALT lengthening<sup>22</sup> therefore the vast majority, if not all tumours, activate  
307 telomerase for telomere maintenance. We did not observe any *TERT* promoter  
308 mutations in our cohort but there are strong negative correlations between methylation  
309 probes in the promoter of *TERT* and tumour TL. This may be a proxy for telomerase  
310 activity since DNA methylation impedes transcription.

311 We see an unexpected divergence between somatic molecular features associated with  
312 TL ratio and those with tumour TL. Specifically, measures of genomic instability are  
313 linked to TL ratio (which represents the ratio between blood TL and tumour TL) while  
314 specific CNAs, GRs, and SNVs are not (**Fig. 1** and **Supplementary Fig. 2**). This  
315 suggests that during the progression of cells from normal to cancerous, non-tumour  
316 (blood) TL may influence tumour genomics, where tumours with shorter TL experience  
317 more genomic instability. Alternatively, a common factor may be influencing during this  
318 epoch of the tumour's evolution. Once tumours are formed, it is the specific mutations  
319 within the cell that are more associated with tumour TL. This may be due to mutations in  
320 cell division and growth regulating genes such as *ATK1* and *SPOP*, which increases the  
321 number of divisions in the tumour and thereby shortens tumour telomeres. Further  
322 evidence of this hypothesis is seen in tumours with *PCAT1* fusions, where tumours with  
323 this fusion had shorter tumour TL than samples without it<sup>39</sup>.

324 One limitation in the estimation of TL using short-read whole genome sequencing is the  
325 difficulty in estimating chromosome specific telomere lengths. Junction spanning reads  
326 from paired-end experiments, in which one read maps within the first or last band of the  
327 chromosome and the other read maps within the telomere region, are scarce. Further  
328 studies should be performed using long read sequences, in which these regions may  
329 have more coverage and can be used to determine chromosome specific shortening  
330 and its association to specific genomic events or biochemical relapse.

331 These data highlight the complicated relationship between telomere length in both  
332 tumour and non-tumour cells, and molecular and clinical tumour phenotypes. They  
333 highlight the need for increased study of telomere length across cancer types, and for  
334 long-read sequencing to introduce chromosome-specific analyses.

## 335 **Acknowledgments**

336 The authors thank all members of the Boutros lab for insightful commentary and  
337 technical support.

## 338 **Funding**

339 This study was conducted with the support of the Ontario Institute for Cancer Research  
340 to PCB through funding provided by the Government of Ontario. This work was  
341 supported by Prostate Cancer Canada and is proudly funded by the Movember  
342 Foundation - Grant #RS2014-01. Dr. Boutros was supported by a Terry Fox Research  
343 Institute New Investigator Award and a CIHR New Investigator Award. This work was  
344 funded by the Government of Canada through Genome Canada and the Ontario  
345 Genomics Institute (OGI-125). This work was supported by the NIH/NCI under award  
346 number P30CA016042, by an operating grant from the National Cancer Institute Early  
347 Detection Research Network (U01CA214194) and by support from the ITCR  
348 (U24CA248265).

## 349 **Author contributions**

350 Formal Analysis: JL. Methodology: JL, ED. Data curation: JL, YSY, TNY, LEH, VH, RL.  
351 Visualization: JL, JG. Supervision: MF., TvdK, RGB, PCB. Conceptualization,  
352 Supervision: PCB, MF, RGB. Pathology Reviews: TvdK. Writing - original draft: JL,  
353 PCB. Writing – review & editing: JL, TNY, VH, RL, MF, PCB. Approved the Manuscript:  
354 All Authors

## 355 **Declaration of Interest and Financial Disclosures**

356 All authors declare that they have no conflicts of interest.

## 357 **Figure Legends**

358 **Figure 1. Tumour telomere length (TL) is associated with genomic features. A,**  
359 Correlation between tumour TL and non-tumour (blood) TL. **B,** Correlation between  
360 tumour TL and TL ratio (tumour TL / non-tumour (blood) TL). **C,** Correlation between  
361 non-tumour (blood) TL and TL ratio. **D,** Tumour TL is ranked in descending order of  
362 length (kbp; top bar plot). The association of tumour TL and measures of mutational  
363 burden, TMRSS2:ERG (T2E) fusion status, as well as known prostate cancer genes  
364 with recurrent CNAs, coding SNVs, and GRs are shown. Bar plots to the right indicate  
365 the statistical significance of each association (see **Methods**).

366 **Figure 2. Mutational landscape differs with telomere length. A-B,** Correlation  
367 between the number of SNVs and **A,** tumour TL and **B,** TL ratio. **C-D,** Correlation  
368 between the number of indels and **C,** tumour TL and **D,** TL ratio. **E-F,** Correlation  
369 between the number of GRs and **E,** and tumour TL and **F,** TL ratio. **G-H,** Correlation of  
370 percentage of the genome altered (PGA) and **G,** tumour TL and **H,** TL ratio. **I-J,**  
371 Correlation between the number of fusions and **I,** tumour TL and **J,** TL ratio. Orange  
372 dots indicate tumour TL while green dots indicate TL ratio. Spearman  $\rho$  and p-values  
373 are displayed.

374 **Figure 3. The genomic correlates of *TERT* abundance. A,** Correlation of *TERT* RNA  
375 abundance with tumour TL and TL ratio. Orange dots indicate tumour TL while green  
376 dots indicate TL ratio. Spearman  $\rho$  and p-values are displayed. **B-E,** Correlation of  
377 *TERT* abundance and **B,** the number of GRs, **C,** number of SNVs, **D,** number of indels,  
378 and **E,** PGA. Spearman  $\rho$  and p-values are displayed. **F,** Spearman's correlation of  
379 significantly associated methylation probes with RNA abundance and tumour TL. Blue  
380 dots indicate a positive correlation while orange dots indicate a negative correlation.  
381 Probes within the promoter are labeled in red while the rest are located in the gene  
382 body. Dot size indicated the magnitude of correlation. Background colour indicates  
383 unadjusted p-values. Methylation probes are ordered by their correlation between *TERT*  
384 RNA abundance from negative to positive.

385 **Figure 4. Association of methylation, RNA abundance, protein abundance and**  
386 **telomere length. A,** Positive correlation of methylation and tumour TL, but negative  
387 correlation of RNA and protein abundance. Top panels in light blue represent  
388 methylation, middle panels in blue-grey represent RNA abundance and the bottom  
389 panels in purple represent protein abundance. Darker purple dots represent undetected,  
390 imputed abundance measures. Spearman  $\rho$  and p-values are displayed. **B,** Negative  
391 correlation of methylation and tumour TL, but positive correlation of RNA and protein  
392 abundance. Top panels in light blue represent methylation, middle panels in blue-grey  
393 represent RNA abundance and the bottom panels in purple represent protein  
394 abundance. Darker purple dots represent undetected, imputed protein abundance  
395 measures. Spearman  $\rho$  and p-values are displayed.

396 **Figure 5. Telomere length differs by copy number status. A,** Difference in tumour  
397 TL between samples with a copy number aberration and those without in prostate  
398 cancer related genes and associated genes. **B,** Difference in TL ratio between samples  
399 with a copy number aberration and those without in prostate cancer related and  
400 associated genes. Q-values are from a Mann-Whitney U test and are bolded when  
401 significant (FDR < 0.05). Colour of the points indicate copy-number status of the gene:  
402 amplification (red), deletion (blue), or neutral (black).

403 **Figure 6. Telomere length is associated with clinical features and biochemical**  
404 **relapse. A-B,** Correlation of age at diagnosis with **A,** tumour TL and **B,** TL ratio.  
405 Spearman  $\rho$  and p-values are displayed. **C-D,** Correlation of pre-treatment PSA with **C,**  
406 tumour TL and **D,** TL ratio. Spearman  $\rho$  and p-values are displayed. **E-F,** Association of  
407 ISUP grade with **E,** tumour TL and **F,** TL ratio. P-value is from an one-way ANOVA. **G-**  
408 **H,** Association of T category with **G,** tumour TL and **H,** TL ratio. P-value is from an one-  
409 way ANOVA. On all plots, green indicates TL ratio, while orange indicates tumour TL. **I-**  
410 **K,** Cox proportional hazard models were created for **I,** non-tumour (blood) TL, **J,** tumour  
411 TL and **K,** TL ratio with BCR as the endpoint. Samples were split into two groups based  
412 on the optimal cut point analysis (see **Methods**).

## 413 **Methods**

### 414 **CPC-GENE patient cohort**

415 Patient selection, tissue collection and sample processing has been previously  
416 described in detail<sup>13</sup>. Briefly, informed consent, consistent with the guidelines of the  
417 local Research Ethics Board (REB) and International Cancer Genome Consortium  
418 (ICGC), was obtained at the time of clinical follow-up. Previously collected tumour  
419 tissues were used, following University Health Network REB-approved study protocols  
420 (UHN 06-0822-CE, UHN 11-0024-CE, CHUQ 2012-913:H12-03-192). All patients were  
421 male and N0M0 as an entry criterion for the study. For RadP patients, BCR was defined  
422 as two consecutive post-RadP PSA measurements of more than 0.2 ng/ml (backdated  
423 to the date of the first increase). If a patient has successful salvage radiation therapy,  
424 this is not BCR. If PSA continues to rise after radiation therapy, BCR is backdated to  
425 first PSA > 0.2. If patient gets other salvage treatment (such as hormones or  
426 chemotherapy), this is considered BCR. Tumour cellularity and Gleason grades were  
427 evaluated independently by two genitourinary pathologists on scanned haematoxylin-  
428 and eosin-stained slides. Serum PSA concentrations (ng/mL) are reported according to  
429 the reading at the time of diagnosis. Cellularity was also determined *in silico* from  
430 OncoScan SNP arrays via qpure (v1.1)<sup>40</sup>.

### 431 **Whole-genome sequencing and data analysis**

432 Whole-genome sequencing was conducted as described before<sup>13</sup>. Briefly, sequencing  
433 libraries were prepared using 50 ng of gDNA and enzymatic reagents from KAPA  
434 Library Preparation Kits (KAPA Biosystems, Woburn, MA USA Cat#KK8201) according  
435 to protocols as described for end repair, A-tailing, and adapter ligation<sup>41</sup>. Sequencing  
436 was carried out on the Illumina HiSeq 2000 platform (Illumina Inc.) and samples were  
437 sequenced to a minimum coverage depth of 50x and 30x for tumour and non-tumour  
438 (blood) samples, respectively.

439 Raw sequencing reads were aligned to the human reference genome, GRCh37, using  
440 BWA-mem (version > 0.7.12; <sup>42</sup> at the lane level. Picard (v1.92;  
441 <http://broadinstitute.github.io/picard/>) was used to merge the lane-level BAMs from the  
442 same library and mark duplicates. Library level BAMs from each sample were also  
443 merged without marking duplicates using Picard. Local realignment and base quality  
444 recalibration was carried out on tumour/non-tumour (blood) pairs together using the  
445 Genome Analysis Toolkit (GATK; > version 3.4.0; <sup>43</sup>. Tumour and non-tumour (blood)  
446 sample level BAMs were extracted, headers were corrected using SAMtools (v0.1.9; <sup>44</sup>,  
447 and files were indexed with Picard (v1.92).

### 448 **Computational telomere length estimation**

449 Tumour and non-tumour (blood) telomere length was estimated using TelSeq (v0.0.1; <sup>23</sup>  
450 and TelomereHunter (v1.0.4)<sup>24</sup> on BAM files generated using bwa-mem (version >

451 0.712; <sup>42</sup> and GATK (version > 3.4.0; <sup>43</sup>. As a quality measure, TelSeq estimates for  
452 each sample were generated per sequencing lane. Reads from lanes that contained too  
453 few reads to calculate an estimate (marked as UNKNOWN), and outlier lanes as  
454 identified by grub's test, were removed from input BAMs using BAMQL v1.6)<sup>45</sup>. After  
455 outliers were removed, TelSeq was run again ignoring read groups with the -u  
456 parameter. Samples with telomere estimates less than one were removed from further  
457 analysis. To account for differences in TL due to sequencing center, a linear model was  
458 fit with TL as the response variable and sequencing center as the predictor variable. A  
459 separate model was fit for tumour and non-tumour (blood) length.

### 460 **Somatic variant calling**

461 Single nucleotide variants (SNVs) and genomic rearrangements (GRs) were called  
462 using pipelines that have been described in detail elsewhere<sup>13</sup>. Briefly, SomaticSniper  
463 (v1.0.5; <sup>46</sup> was used to call SNVs on bases with at least 17x coverage in tumours and  
464 10x in non-tumours (blood). Coding versus non-coding SNVs were determined using  
465 Annovar<sup>47</sup>. Genomic rearrangements were identified using Delly (version 0.7.8; <sup>48</sup>. Gene  
466 fusion events involving *ERG* or *ETV* were collectively referred to as ETS events.  
467 Genomic rearrangement calls were examined to determine if breakpoints led to a  
468 TMPRSS2:ERG fusion or if breakpoints were found in both 1 Mbp bins surrounding the  
469 following gene pairs: *ERG:SLC45A3*, *ERG:NDRG1*, *ETV1:TMPRSS2*,  
470 *ETV4:TMPRSS2*, *ETV1:SLC45A3*, *ETV4:SLC45A3*, *ETV1:NDRG1*, and *ETV4:NDRG1*.  
471 *ERG* immunohistochemistry and deletion calls between *TMPRSS2* and *ERG* loci in  
472 OncoScan SNP array data provided further support for these fusions.

### 473 **mRNA abundance data generation and analysis**

474 Generation and analysis of mRNA abundance data has been previously described in  
475 detail<sup>13</sup>. Briefly, total RNA was extracted using the mirVana miRNA Isolation Kit (Life  
476 Technologies), according to the manufacturer's instructions. 100-150 ng of total RNA  
477 was assayed on the Human Gene 2.0 ST array or the Affymetrix Human Transcriptome  
478 Array 2.0. Background correction, normalization and annotation were carried out using  
479 the oligo (v1.34.2) package. The robust multichip average (RMA) algorithm was applied  
480 to the raw intensity data<sup>49</sup>. Probes were mapped to Entrez gene IDs using custom CDF  
481 files (v20) for HTA 2.0 and HuGene 2.0 ST array.

### 482 **Methylation microarray data generation**

483 Illumina Infinium HumanMethylation 450k BeadChip kits were used to assess global  
484 methylation, using 500 ng of input genomic DNA, at McGill University and the Genome  
485 Quebec Innovation Centre (Montreal, QC). All samples used in this study were  
486 processed from fresh-frozen prostate cancer tissue. The IDAT files were loaded and  
487 converted to raw intensity values with the use of watermelon package (v1.15.1; <sup>50</sup>.  
488 Quality control was conducted using the minfi package (v1.22.1; <sup>51</sup>; no outlier samples  
489 were detected). Raw methylation intensity levels were then pre-processed using Dasen.

490 Probe filtering was conducted after normalization, as previously described<sup>13</sup>. Annotation  
491 to chromosome location, probe position, and gene symbol was conducted using the  
492 IlluminaHumanMethylation450kanno.ilmn12.hg19 package (v0.6.0).

### 493 **Association of telomere length with chromothripsis**

494 Chromothripsis scores were previously generated using ShatterProof (v0.14; <sup>13,25</sup> with  
495 default settings. Spearman's correlation between the maximum ShatterProof score per  
496 sample and telomere length was calculated using samples with both available metrics  
497 (n = 170).

498

### 499 **Association of telomere length with clinical and genomic features**

500 Telomere length estimates were associated with genomic and clinical features. Clinical  
501 features, including ISUP Grade, pre-treatment PSA, T category and age at diagnosis,  
502 were categorized and tested for association using an one-way ANOVA. Pathological T  
503 category was used for surgery samples and diagnostic T category was used for  
504 radiotherapy samples. Binary features including the presence of specific GRs, CNAs  
505 and SNVs were tested for association using a Mann-Whitney U test. Summary features  
506 including PGA, GR count, SNV count and indel count were correlated to TL using  
507 Spearman's correlation.

### 508 **Association of telomere length with methylation**

509 The correlation matrix of methylation and mRNA abundance levels from TCGA was  
510 downloaded from <https://gdac.broadinstitute.org/>. For each gene, the probe showing the  
511 highest Spearman's correlation with mRNA abundance levels was used in our  
512 correlation analysis.

### 513 **Association of telomere length with transcriptome abundance**

514 Spearman's correlations between RNA abundance (n = 139; <sup>13</sup> and TL, as well as,  
515 protein abundance (n = 70; <sup>16</sup> and TL were calculated. Pathway analysis was performed  
516 with g:ProfileR<sup>32</sup> using genes that were significantly negatively or positively correlated to  
517 TL.

### 518 **Association of telomere length with copy number aberrations**

519 Microarray data generation and analysis has been previously described in detail<sup>13</sup>.  
520 Briefly, SNP microarrays were performed with 200 ng of DNA on Affymetrix OncoScan  
521 FFPE Express 2.0 and 3.0 arrays. Analysis of the probe assays was performed using  
522 .OSCHP files generated by OncoScan Console (v1.1) using a custom reference.  
523 BioDiscovery's Nexus Express<sup>TM</sup> for OncoScan 3 Software was used to call copy  
524 number aberrations using the SNP-FASST2 algorithm. Gene level copy number  
525 aberrations for each patient were identified by overlapping copy number segments from  
526 OncoScan SNP 3.0 data, with RefGene (2014-07-15) annotation using BEDTools  
527 (v2.17.0; <sup>52</sup>. Genes with the same copy number profile across patients were then  
528 collapsed into contiguous regions. Contiguous gene segments with aberrations in less



529 that 5% of patients were removed from the analysis. To find associations between TL  
530 and copy number segments, a Mann-Whitney U test was used to compare the mean TL  
531 between samples with a copy number aberration and those without. P-values were FDR  
532 adjusted to account for multiple testing.

### 533 **Association with biochemical relapse**

534 Cox proportional hazards models were fit with the R package survival (v3.2-7) using TL  
535 as a continuous variable. Age at diagnosis was controlled for in the model. Kaplan  
536 Meier plots were generated by dichotomizing samples based on the optimal cut point  
537 analysis, in which samples were dichotomized using increasing thresholds of 50 bp.

### 538 **Statistical analyses and data visualization**

539 All statistical analyses were performed within the R statistical environment (v3.3.1).  
540 Visualization in R was performed through the BoutrosLab Plotting General package  
541 (v5.6.1; <sup>53</sup>).

### 542 **Data availability**

543 OncoScan SNP array data and whole genome DNA sequencing can be found on EGA  
544 under the accession EGAS00001000900. Processed variant calls are available through  
545 the ICGC Data Portal under the project PRAD-CA ([https://dcc.icgc.org/projects/PRAD-  
546 CA](https://dcc.icgc.org/projects/PRAD-CA)). mRNA data is available in the Gene Expression Omnibus under the accession  
547 GSE84043. Methylation data is available under the accession GSE107298.

## 548 **Supplementary Table Legends**

### 549 **Supplementary Table 1 | Clinical and Genomic Features of Tumours**

550 Clinical data for 382 samples used in analysis after applying quality control metrics.

### 551 **Supplementary Table 2 | Association between Tumour TL and 552 recurrent gene fusions**

553 Statistical summary of 47 recurrent fusions pairs tested for association with TL using a  
554 Wilcoxon signed-rank test.

### 555 **Supplementary Table 3 | Genomic and transcriptomic correlations 556 with Tumour TL**

557 Results from Spearman's correlation between tumour TL and methylation beta values,  
558 RNA abundance and protein abundance. Q-values are FDR adjusted P-values. NAs  
559 indicate missing values where tests could not be performed.

### 560 **Supplementary Table 4 | Genomic and transcriptomic correlations 561 with TL ratio**

562 Results from Spearman's correlation between tumour TL and methylation beta values,  
563 RNA abundance and protein abundance. Q-values are FDR adjusted P-values. NAs  
564 indicate missing values where tests could not be performed.

### 565 **Supplementary Table 5 | Associations between CNAs and Tumour TL**

566 Associations between CNAs and Tumour TL, ordered by FDR adjusted P-values. Each  
567 row represents collapsed segments containing multiple genes. Contiguous gene  
568 segments with aberrations in less that 5% of patients were removed.

### 569 **Supplementary Table 6 | Associations between CNAs and TL ratio**

570 Statistically significant associations between CNAs and TL ratio, ordered by FDR  
571 adjusted P-values. Each row represents collapsed segments containing multiple genes.  
572 Contiguous gene segments with aberrations in less that 5% of patients were removed.

## 573 **References**

- 574 1. Moyzis RK, Buckingham JM, Cram LS, et al. A highly conserved repetitive DNA  
575 sequence, (TTAGGG)<sub>n</sub>, present at the telomeres of human chromosomes. *Proc*  
576 *Natl Acad Sci USA*. 1988;85(18):6622-6626.
- 577 2. Arnoult N, Karlseder J. Complex interactions between the DNA-damage response  
578 and mammalian telomeres. *Nat Struct Mol Biol*. 2015;22(11):859-866.  
579 doi:10.1038/nsmb.3092
- 580 3. Samassekou O, Gadji M, Drouin R, Yan J. Sizing the ends: normal length of human  
581 telomeres. *Ann Anat*. 2010;192(5):284-291. doi:10.1016/j.aanat.2010.07.005
- 582 4. Hayflick L, Moorhead PS. The serial cultivation of human diploid cell strains. *Exp*  
583 *Cell Res*. 1961;25:585-621.
- 584 5. Hanahan D, Weinberg RA. The hallmarks of cancer. *Cell*. 2000;100(1):57-70.
- 585 6. Dunham MA, Neumann AA, Fasching CL, Reddel RR. Telomere maintenance by  
586 recombination in human cells. *Nat Genet*. 2000;26(4):447-450. doi:10.1038/82586
- 587 7. Barthel FP, Wei W, Tang M, et al. Systematic analysis of telomere length and  
588 somatic alterations in 31 cancer types. *Nat Genet*. 2017;49(3):349-357.  
589 doi:10.1038/ng.3781
- 590 8. Sieverling L, Hong C, Koser SD, et al. Genomic footprints of activated telomere  
591 maintenance mechanisms in cancer. *Nature Communications*. 2020;11(1):733.  
592 doi:10.1038/s41467-019-13824-9
- 593 9. Lalonde E, Ishkanian AS, Sykes J, et al. Tumour genomic and microenvironmental  
594 heterogeneity for integrated prediction of 5-year biochemical recurrence of prostate  
595 cancer: a retrospective cohort study. *Lancet Oncol*. 2014;15(13):1521-1532.  
596 doi:10.1016/S1470-2045(14)71021-6
- 597 10. Lalonde E, Alkallas R, Chua MLK, et al. Translating a Prognostic DNA Genomic  
598 Classifier into the Clinic: Retrospective Validation in 563 Localized Prostate  
599 Tumors. *European Urology*. 2017;72(1):22-31. doi:10.1016/j.eururo.2016.10.013
- 600 11. Baca SC, Prandi D, Lawrence MS, et al. Punctuated evolution of prostate cancer  
601 genomes. *Cell*. 2013;153(3):666-677. doi:10.1016/j.cell.2013.03.021
- 602 12. The Cancer Genome Atlas Research Network. The molecular taxonomy of primary  
603 prostate cancer. *Cell*. 2015;163(4):1011-1025. doi:10.1016/j.cell.2015.10.025
- 604 13. Fraser M, Sabelnykova VY, Yamaguchi TN, et al. Genomic hallmarks of localized,  
605 non-indolent prostate cancer. *Nature*. 2017;541(7637):359-364.  
606 doi:10.1038/nature20788

- 607 14. Bhandari V, Hoey C, Liu LY, et al. Molecular landmarks of tumor hypoxia across  
608 cancer types. *Nature Genetics*. Published online January 14, 2019:1.  
609 doi:10.1038/s41588-018-0318-2
- 610 15. Espiritu SMG, Liu LY, Rubanova Y, et al. The Evolutionary Landscape of Localized  
611 Prostate Cancers Drives Clinical Aggression. *Cell*. 2018;173(4):1003-1013.e15.  
612 doi:10.1016/j.cell.2018.03.029
- 613 16. Sinha A, Huang V, Livingstone J, et al. The Proteogenomic Landscape of Curable  
614 Prostate Cancer. *Cancer Cell*. 2019;35(3):414-427.e6.  
615 doi:10.1016/j.ccell.2019.02.005
- 616 17. Chen S, Huang V, Xu X, et al. Widespread and Functional RNA Circularization in  
617 Localized Prostate Cancer. *Cell*. 2019;176(4):831-843.e22.  
618 doi:10.1016/j.cell.2019.01.025
- 619 18. Ciriello G, Miller ML, Aksoy BA, Senbabaoglu Y, Schultz N, Sander C. Emerging  
620 landscape of oncogenic signatures across human cancers. *Nat Genet*.  
621 2013;45(10):1127-1133. doi:10.1038/ng.2762
- 622 19. Robinson D, Van Allen EM, Wu Y-M, et al. Integrative clinical genomics of  
623 advanced prostate cancer. *Cell*. 2015;161(5):1215-1228.  
624 doi:10.1016/j.cell.2015.05.001
- 625 20. Kim H, Chen J. c-Myc interacts with TRF1/PIN2 and regulates telomere length.  
626 *Biochem Biophys Res Commun*. 2007;362(4):842-847.  
627 doi:10.1016/j.bbrc.2007.08.064
- 628 21. Lee SS, Bohrson C, Pike AM, Wheelan SJ, Greider CW. ATM Kinase Is Required  
629 for Telomere Elongation in Mouse and Human Cells. *Cell Rep*. 2015;13(8):1623-  
630 1632. doi:10.1016/j.celrep.2015.10.035
- 631 22. Sommerfeld HJ, Meeker AK, Piatyszek MA, Bova GS, Shay JW, Coffey DS.  
632 Telomerase activity: a prevalent marker of malignant human prostate tissue.  
633 *Cancer Res*. 1996;56(1):218-222.
- 634 23. Ding Z, Mangino M, Aviv A, Spector T, Durbin R, UK10K Consortium. Estimating  
635 telomere length from whole genome sequence data. *Nucleic Acids Res*.  
636 2014;42(9):e75. doi:10.1093/nar/gku181
- 637 24. Feuerbach L, Sieverling L, Deeg KI, et al. TelomereHunter – in silico estimation of  
638 telomere content and composition from cancer genomes. *BMC Bioinformatics*.  
639 2019;20(1):272. doi:10.1186/s12859-019-2851-0
- 640 25. Govind SK, Zia A, Hennings-Yeomans PH, et al. ShatterProof: operational  
641 detection and quantification of chromothripsis. *BMC Bioinformatics*. 2014;15:78.  
642 doi:10.1186/1471-2105-15-78

- 643 26. Chin L, Artandi SE, Shen Q, et al. p53 deficiency rescues the adverse effects of  
644 telomere loss and cooperates with telomere dysfunction to accelerate  
645 carcinogenesis. *Cell*. 1999;97(4):527-538.
- 646 27. Maciejowski J, Li Y, Bosco N, Campbell PJ, de Lange T. Chromothripsis and  
647 Kataegis Induced by Telomere Crisis. *Cell*. 2015;163(7):1641-1654.  
648 doi:10.1016/j.cell.2015.11.054
- 649 28. Armenia J, Wankowicz SAM, Liu D, et al. The long tail of oncogenic drivers in  
650 prostate cancer. *Nat Genet*. 2018;50(5):645-651. doi:10.1038/s41588-018-0078-z
- 651 29. Heaphy CM, de Wilde RF, Jiao Y, et al. Altered telomeres in tumors with ATRX and  
652 DAXX mutations. *Science*. 2011;333(6041):425. doi:10.1126/science.1207313
- 653 30. Graham MK, Meeker A. Telomeres and telomerase in prostate cancer development  
654 and therapy. *Nat Rev Urol*. 2017;14(10):607-619. doi:10.1038/nrurol.2017.104
- 655 31. Majumder PK, Sellers WR. Akt-regulated pathways in prostate cancer. *Oncogene*.  
656 2005;24(50):7465-7474. doi:10.1038/sj.onc.1209096
- 657 32. Reimand J, Arak T, Adler P, et al. g:Profiler-a web server for functional  
658 interpretation of gene lists (2016 update). *Nucleic Acids Res*. 2016;44(W1):W83-  
659 89. doi:10.1093/nar/gkw199
- 660 33. Weischenfeldt J, Simon R, Feuerbach L, et al. Integrative genomic analyses reveal  
661 an androgen-driven somatic alteration landscape in early-onset prostate cancer.  
662 *Cancer Cell*. 2013;23(2):159-170. doi:10.1016/j.ccr.2013.01.002
- 663 34. Heaphy CM, Yoon GS, Peskoe SB, et al. Prostate cancer cell telomere length  
664 variability and stromal cell telomere length as prognostic markers for metastasis  
665 and death. *Cancer Discov*. 2013;3(10):1130-1141. doi:10.1158/2159-8290.CD-13-  
666 0135
- 667 35. Svenson U, Roos G, Wikström P. Long leukocyte telomere length in prostate  
668 cancer patients at diagnosis is associated with poor metastasis-free and cancer-  
669 specific survival. *Tumour Biol*. 2017;39(2):1010428317692236.  
670 doi:10.1177/1010428317692236
- 671 36. Renner W, Krenn-Pilko S, Gruber H-J, Herrmann M, Langsenlehner T. Relative  
672 telomere length and prostate cancer mortality. *Prostate Cancer Prostatic Dis*.  
673 2018;21(4):579-583. doi:10.1038/s41391-018-0068-3
- 674 37. Koeneman KS, Pan CX, Jin JK, et al. Telomerase activity, telomere length, and  
675 DNA ploidy in prostatic intraepithelial neoplasia (PIN). *J Urol*. 1998;160(4):1533-  
676 1539.

- 677 38. Zhang W, Kapusta LR, Slingerland JM, Klotz LH. Telomerase activity in prostate  
678 cancer, prostatic intraepithelial neoplasia, and benign prostatic epithelium. *Cancer*  
679 *Res.* 1998;58(4):619-621.
- 680 39. Prensner JR, Chen W, Iyer MK, et al. PCAT-1, a long noncoding RNA, regulates  
681 BRCA2 and controls homologous recombination in cancer. *Cancer Res.*  
682 2014;74(6):1651-1660. doi:10.1158/0008-5472.CAN-13-3159
- 683 40. Song S, Nones K, Miller D, et al. qpure: A tool to estimate tumor cellularity from  
684 genome-wide single-nucleotide polymorphism profiles. *PLoS ONE.*  
685 2012;7(9):e45835. doi:10.1371/journal.pone.0045835
- 686 41. Fisher S, Barry A, Abreu J, et al. A scalable, fully automated process for  
687 construction of sequence-ready human exome targeted capture libraries. *Genome*  
688 *Biol.* 2011;12(1):R1. doi:10.1186/gb-2011-12-1-r1
- 689 42. Li H, Durbin R. Fast and accurate short read alignment with Burrows-Wheeler  
690 transform. *Bioinformatics.* 2009;25(14):1754-1760.  
691 doi:10.1093/bioinformatics/btp324
- 692 43. McKenna A, Hanna M, Banks E, et al. The Genome Analysis Toolkit: a MapReduce  
693 framework for analyzing next-generation DNA sequencing data. *Genome Res.*  
694 2010;20(9):1297-1303. doi:10.1101/gr.107524.110
- 695 44. Li H, Handsaker B, Wysoker A, et al. The Sequence Alignment/Map format and  
696 SAMtools. *Bioinformatics.* 2009;25(16):2078-2079.  
697 doi:10.1093/bioinformatics/btp352
- 698 45. Masella AP, Lalansingh CM, Sivasundaram P, Fraser M, Bristow RG, Boutros PC.  
699 BAMQL: a query language for extracting reads from BAM files. *BMC*  
700 *Bioinformatics.* 2016;17:305. doi:10.1186/s12859-016-1162-y
- 701 46. Larson DE, Harris CC, Chen K, et al. SomaticSniper: identification of somatic point  
702 mutations in whole genome sequencing data. *Bioinformatics.* 2012;28(3):311-317.  
703 doi:10.1093/bioinformatics/btr665
- 704 47. Wang K, Li M, Hakonarson H. ANNOVAR: functional annotation of genetic variants  
705 from high-throughput sequencing data. *Nucleic Acids Res.* 2010;38(16):e164.  
706 doi:10.1093/nar/gkq603
- 707 48. Rausch T, Zichner T, Schlattl A, Stütz AM, Benes V, Korbel JO. DELLY: structural  
708 variant discovery by integrated paired-end and split-read analysis. *Bioinformatics.*  
709 2012;28(18):i333-i339. doi:10.1093/bioinformatics/bts378
- 710 49. Irizarry RA, Bolstad BM, Collin F, Cope LM, Hobbs B, Speed TP. Summaries of  
711 Affymetrix GeneChip probe level data. *Nucleic Acids Res.* 2003;31(4):e15.

- 712 50. Pidsley R, Y Wong CC, Volta M, Lunnon K, Mill J, Schalkwyk LC. A data-driven  
713 approach to preprocessing Illumina 450K methylation array data. *BMC Genomics*.  
714 2013;14:293. doi:10.1186/1471-2164-14-293
- 715 51. Aryee MJ, Jaffe AE, Corrada-Bravo H, et al. Minfi: a flexible and comprehensive  
716 Bioconductor package for the analysis of Infinium DNA methylation microarrays.  
717 *Bioinformatics*. 2014;30(10):1363-1369. doi:10.1093/bioinformatics/btu049
- 718 52. Quinlan AR, Hall IM. BEDTools: a flexible suite of utilities for comparing genomic  
719 features. *Bioinformatics*. 2010;26(6):841-842. doi:10.1093/bioinformatics/btq033
- 720 53. P'ng C, Green J, Chong LC, et al. BPG: Seamless, automated and interactive  
721 visualization of scientific data. *BMC Bioinformatics*. 2019;20(1):42.  
722 doi:10.1186/s12859-019-2610-2

723

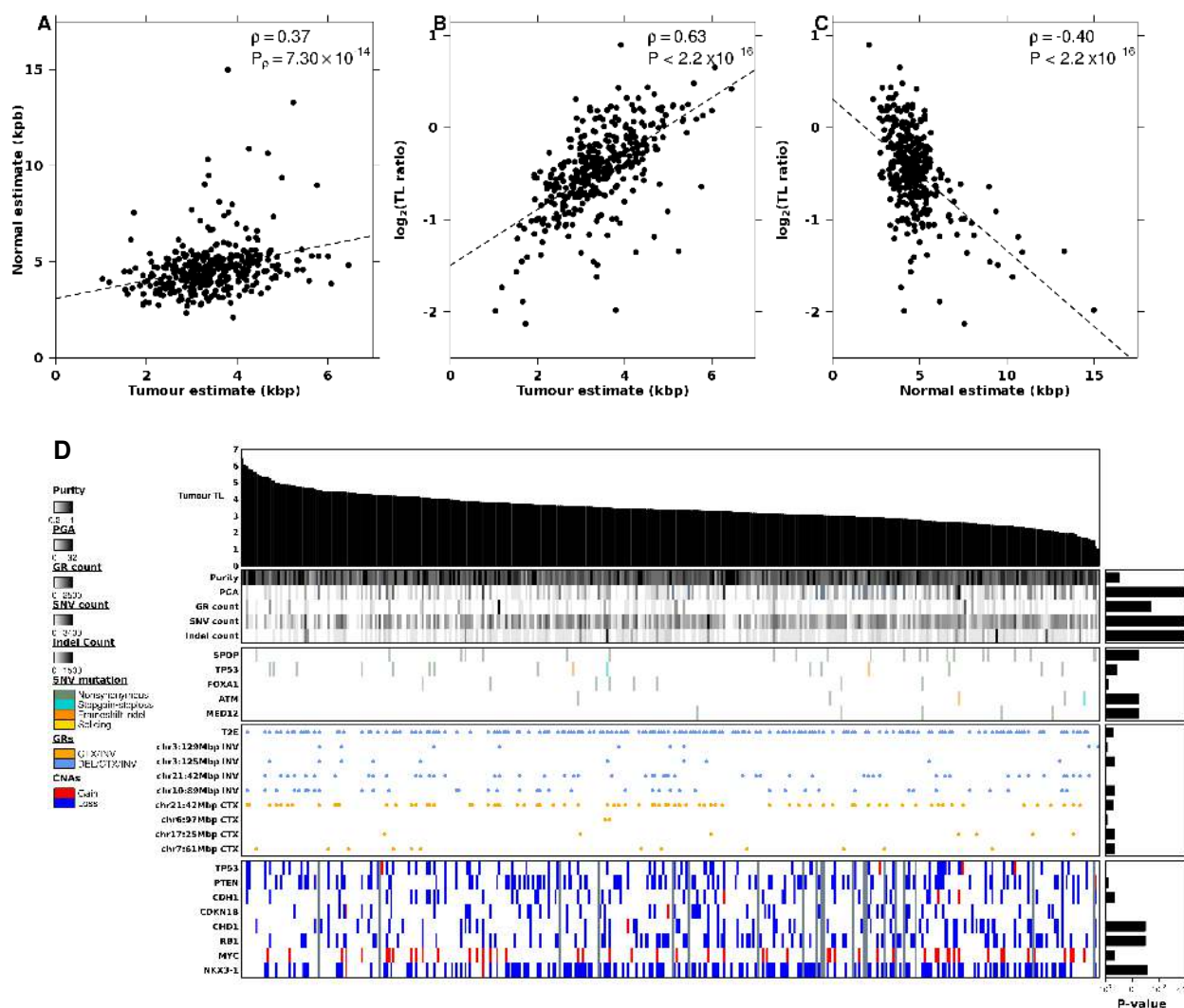


**Figure 1 — Tumour telomere length (TL) is associated with genomic features**

**A-B**, Correlation between tumour TL and **A** non-tumour (blood) TL and **B**, TL ratio (tumour TL / non-tumour (blood) TL). **C**, Correlation between non-tumour (blood) TL and TL ratio. **D**, Tumour TL is ranked in descending order of length (kbp; top bar plot). The association of tumour TL and measures of mutational burden, TMPRSS2:ERG (T2E) fusion status, as well as known prostate cancer genes with recurrent CNAs, coding SNVs, and GRs are shown. Bar plots to the right indicate the statistical significance of each association (see Methods).



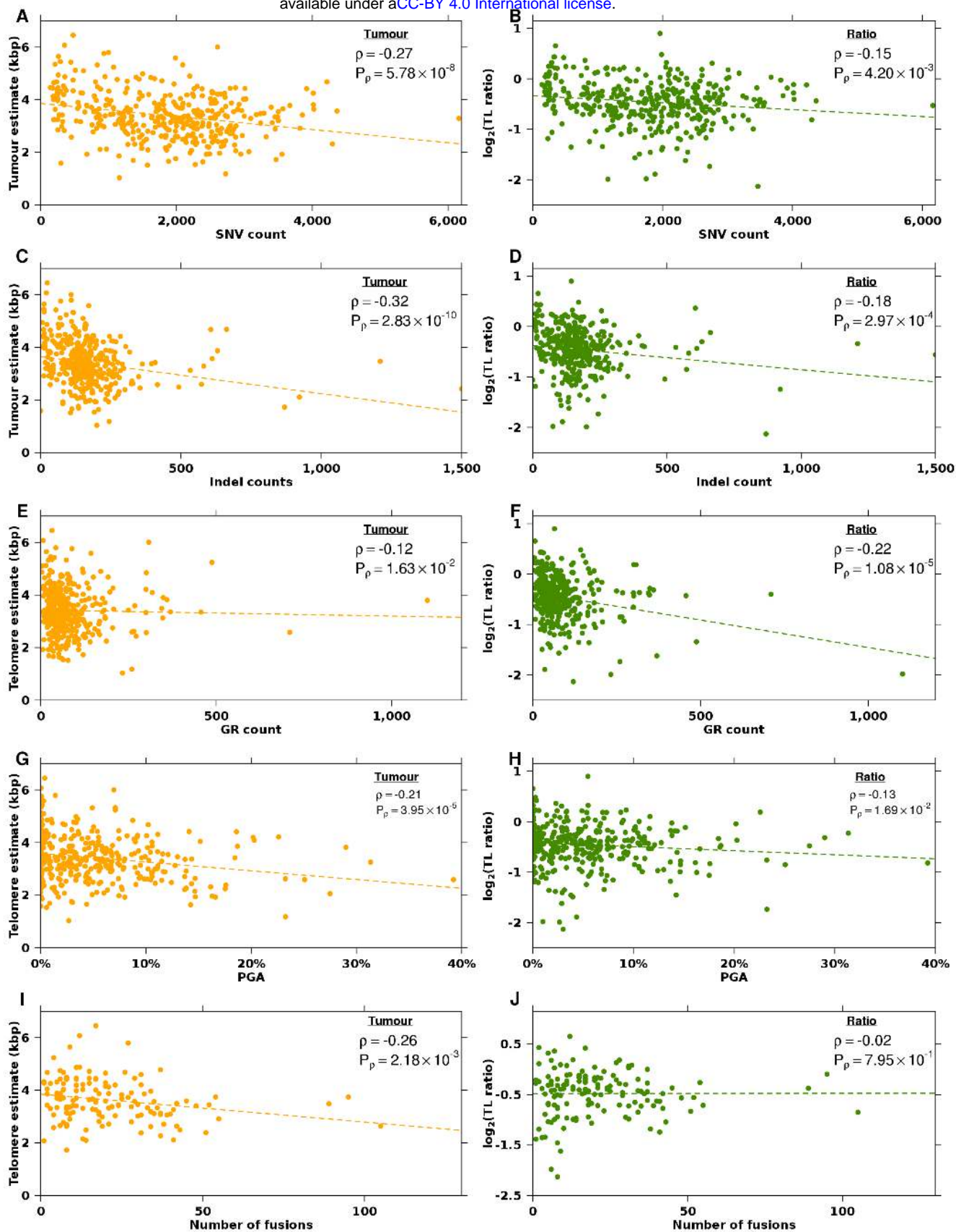


**Figure 2 — Mutational landscape differs with telomere length**

**A-B**, Correlation between the number of SNVs and **A**, tumour TL and **B**, TL ratio. **C-D**, Correlation between the number of indels and **C**, tumour TL and **D**, TL ratio. **E-F**, Correlation between the number of GRs and **E**, and tumour TL and **F**, TL ratio. **G-H**, Correlation of percentage of the genome altered (PGA) and **G**, tumour TL and **H**, TL ratio. **I-J**, Correlation between the number of fusions and **I**, tumour TL and **J**, TL ratio. Orange dots indicate tumour TL while green dots indicate TL ratio. Spearman's  $\rho$  and P-values are displayed.

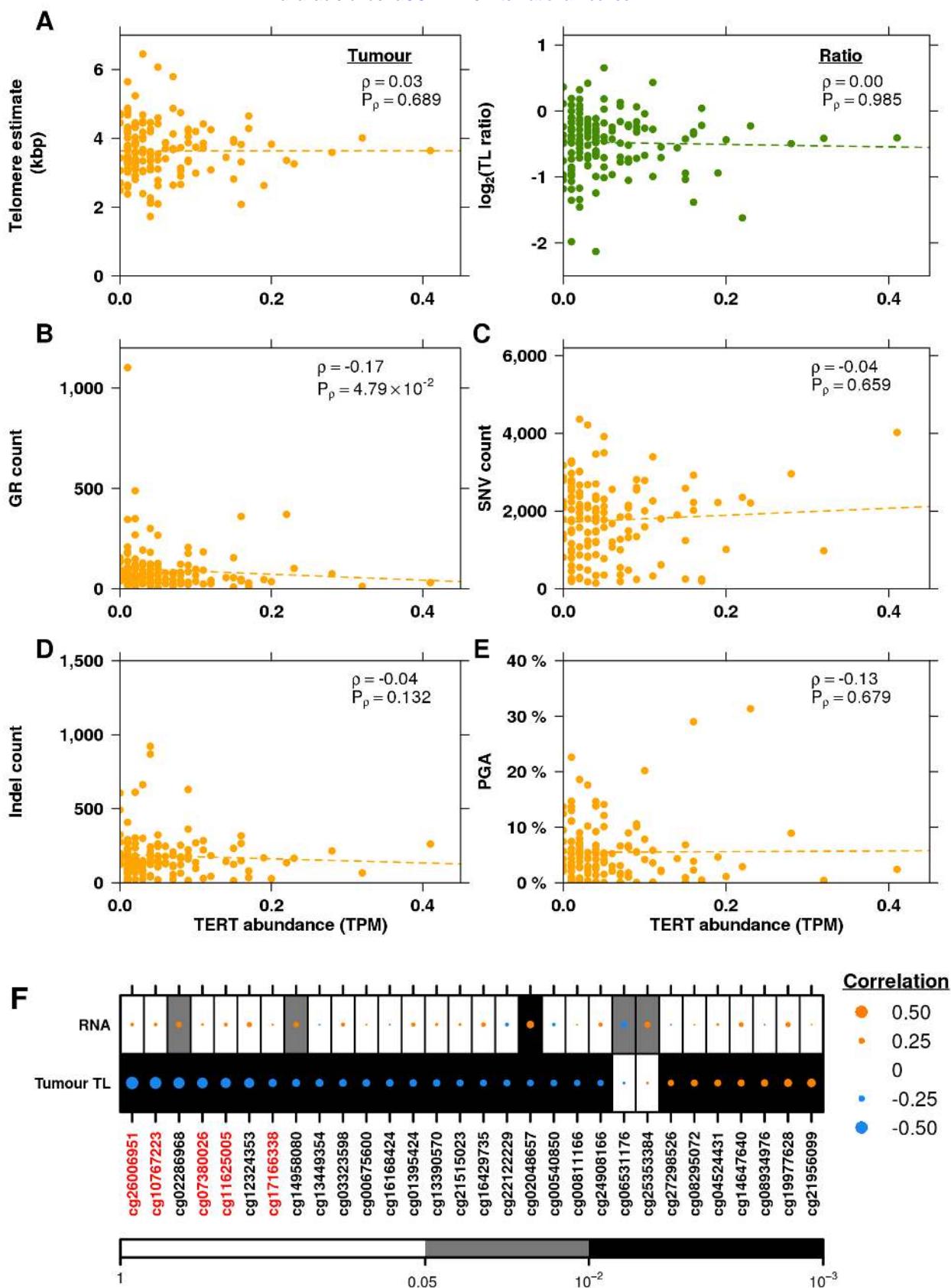


**Figure 3 — The genomic correlates of TERT abundance**

**A**, Correlation of *TERT* RNA abundance with tumour TL and TL ratio. Orange dots indicate tumour TL while green dots indicate TL ratio. Spearman  $\rho$  and P-values are displayed. **B-E**, Correlation of *TERT* abundance and **B**, the number of GRs, **C**, number of SNVs, **D**, number of indels, and **E**, PGA. Spearman  $\rho$  and P-values are displayed. **F**, Spearman's correlation of significantly associated methylation probes with RNA abundance and tumour TL. Orange dots indicate a positive correlation while blue dots indicate a negative correlation. Dot size indicated the magnitude of correlation. Background colour indicates unadjusted P-values. Methylation probes are ordered by their correlation between *TERT* RNA abundance from negative to positive.

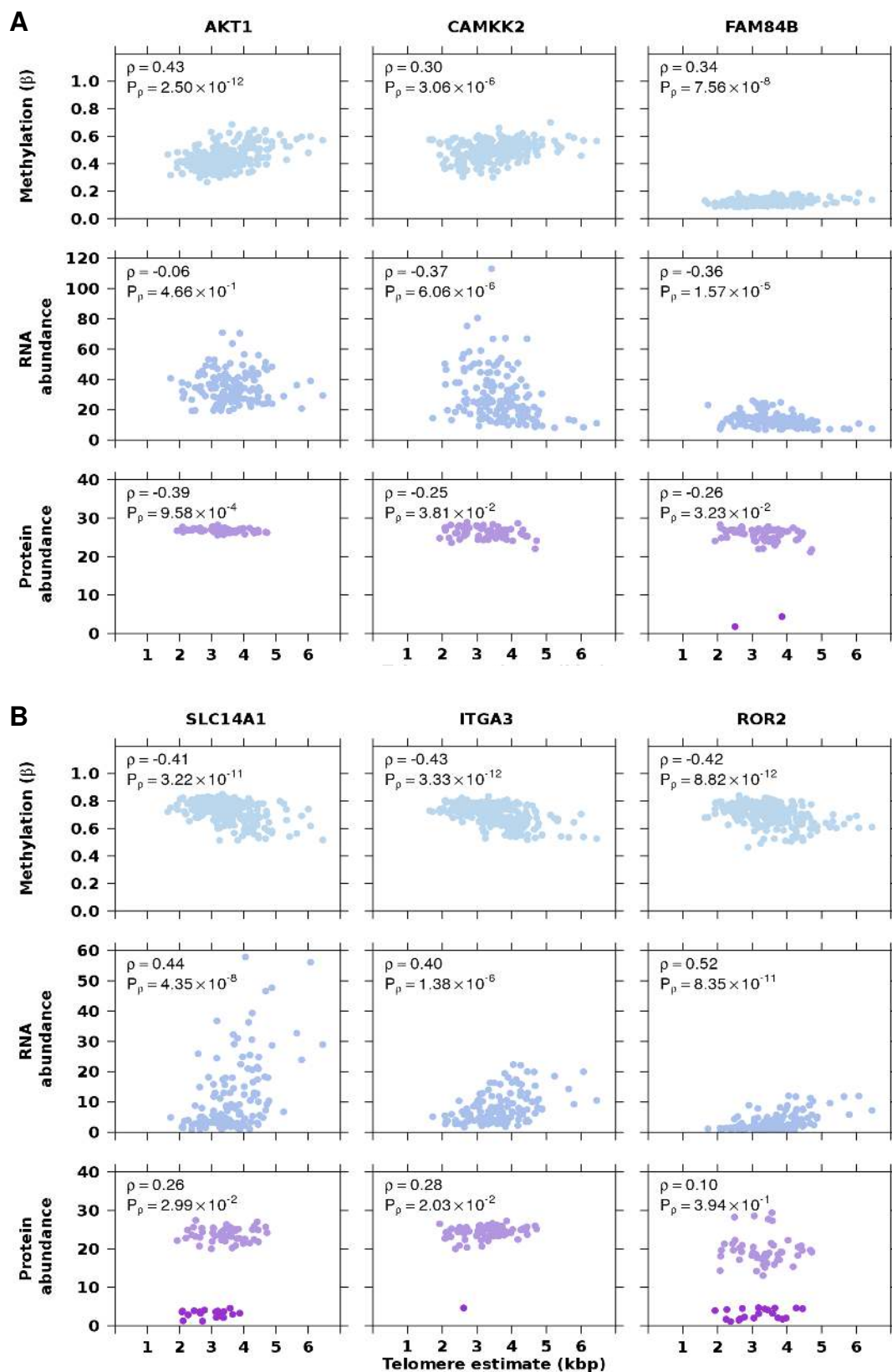


**Figure 4 — Association of methylation, RNA abundance, protein abundance and telomere length**

**A**, Positive correlation of methylation and tumour TL, but negative correlation of RNA and protein abundance. **B**, Negative correlation of methylation and tumour TL, but positive correlation of RNA and protein abundance. Top panels in light blue represent methylation beta values, middle panels in blue-grey represent RNA abundance and the bottom panels in purple represent protein abundance. Darker purple dots represent undetected, imputed protein abundance measures. Spearman  $\rho$  and P-values are displayed.

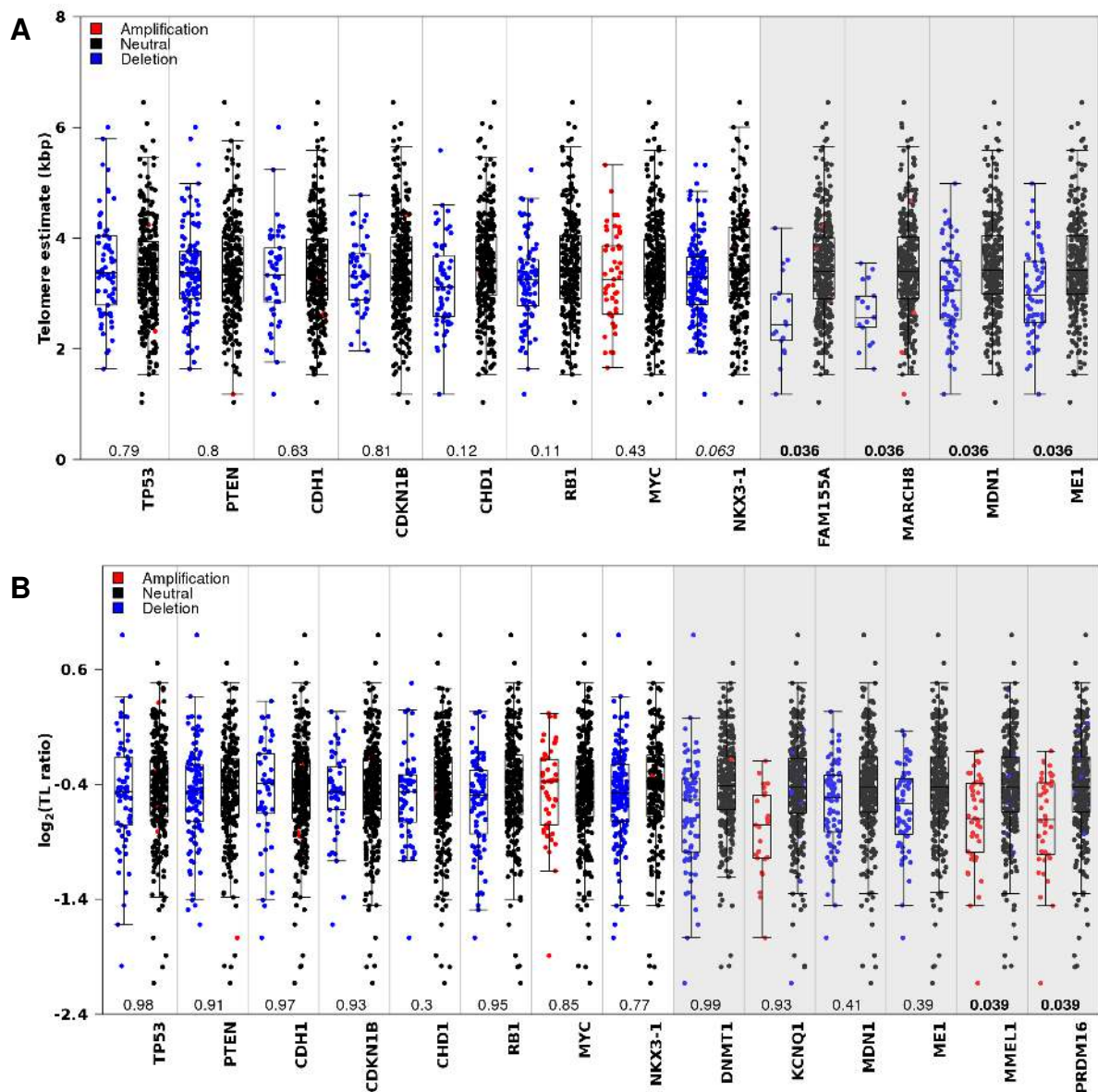


**Figure 5 — Telomere length differs by copy number status**

**A**, Difference in tumour TL between samples with a copy number aberration and those without in prostate cancer related genes and associated genes. **B**, Difference in TL ratio between samples with a copy number aberration and those without in prostate cancer related and associated genes. Q-values are from a Mann-Whitney U test and are bolded when significant ( $< 0.05$ ). Colour of the dots indicate copy number status of the gene: amplification (red), deletion (blue), or neutral (black). Boxes with a white background are known prostate cancer genes, while boxes with a gray background were identified by a genome wide search.

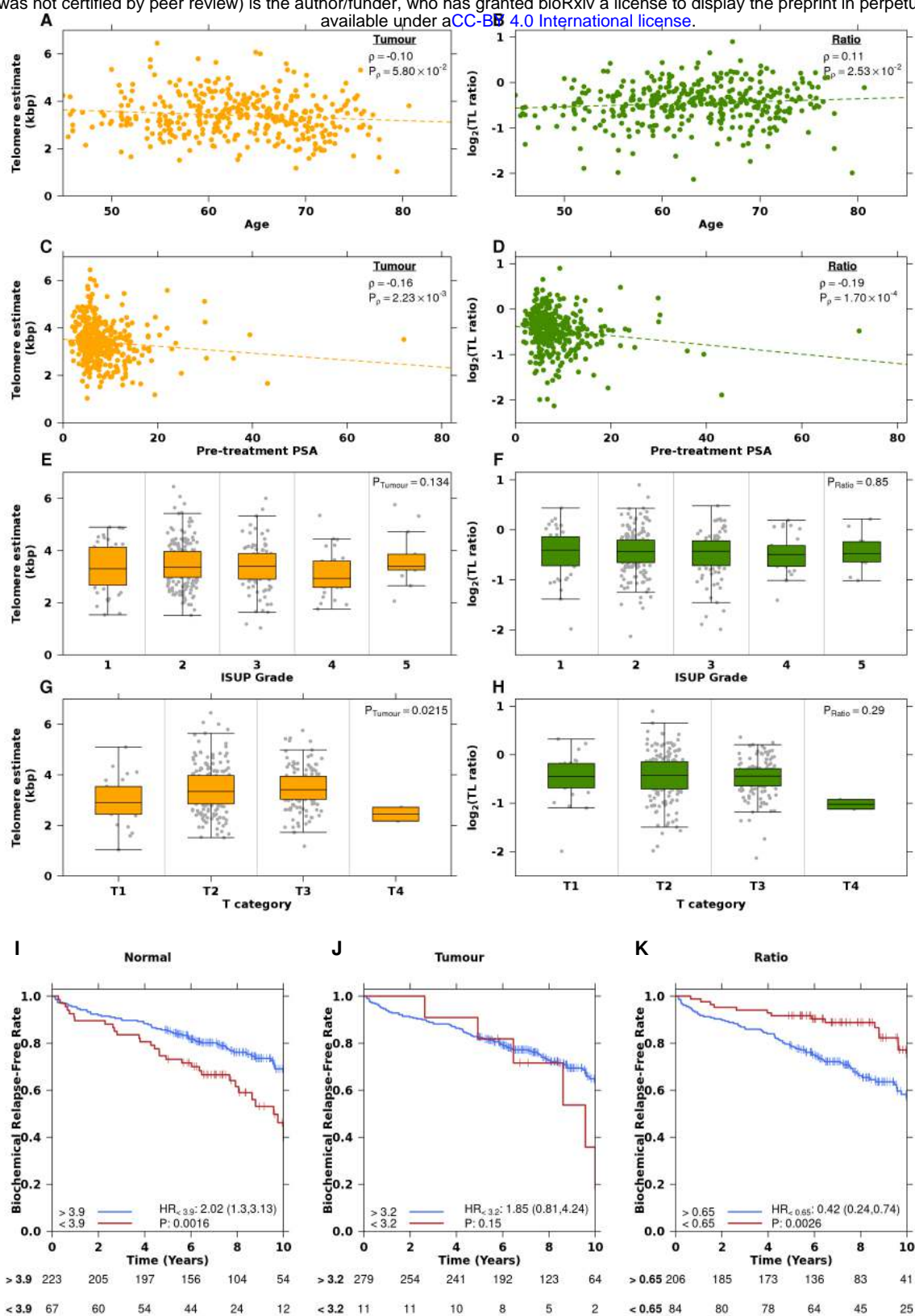


**Figure 6 — Telomere length is associated with clinical features and biochemical relapse**

**A-B**, Correlation of age at treatment with **A**, tumour TL and **B**, TL ratio. Spearman  $\rho$  and P-values are displayed. **C-D**, Correlation of pre-treatment PSA with **C**, tumour TL and **D**, TL ratio. Spearman  $\rho$  and P-values are displayed. **E-F**, Association of ISUP grade with **E**, tumour TL and **F**, TL ratio. P-value is from an one-way ANOVA. **G-H**, Association of T category with **G**, tumour TL and **H**, TL ratio. P-value is from an one-way ANOVA. On all plots, green indicates TL ratio, while orange indicates tumour TL. **I-K**, Cox proportional hazard models were created for **I**, non-tumour (blood) TL, **J**, tumour TL and **K**, TL ratio with BCR as the endpoint. Samples were split into two groups based on the optimal cut point analysis (see **Methods**).